AIAA SciTech Forum
6-10 January 2020, Orlando, FL
AIAA Scitech 2020 Forum

10.2514/6.2020-0047

Analysis of Micro-compressor Performance with Integrated Co-flow Jet Airfoil Ducting System

Kewei Xu, * Brendan McBreen, † Yan Ren, ‡ Gecheng Zha, §
Dept. of Mechanical and Aerospace Engineering
University of Miami, Coral Gables, Florida 33124
E-mail: gzha@miami.edu

Abstract

This paper numerically studies the micro-compressor performance with integrated co-flow jet (CFJ) airfoil injection and suction ducts to mimic the wind tunnel testing condition. The simulation is conducted using 3D Reynolds Averaged Navier-Stokes (RANS) solver and the k-ϵ turbulent model. The boundary conditions from the wind tunnel testing are used to simulate the experimental conditions. Five RPMs of the micro-compressor are simulated. The predicted static pressure ratio achieves a very good agreement with the experiment measurements with the maximum discrepancy less than 3%. The results indicate that the micro-compressor is operated at an operating line that is shifted from the design operating line with substantially lower pressure ratio. This is because that the static pressure at the CFJ airfoil injection area near leading edge is very low due to the very strong suction effect caused by the CFJ injection effect. Working at the off-design condition decreases the compressor efficiency from the designed value of 80% to about 25%. This off-design operation is because the CFJ airfoil with the injection/suction ducts and the micro-compressors are designed with a loose integration, which creates the mismatch between the compressor provided back pressure and the static pressure required by the CFJ injection duct outlet. The micro-compressor is over-designed to have a too high back pressure at the design point. This study is an important step to develop an integrated design process with micro-compressors, the injection and suction ducts, and the CFJ airfoil to avoid the pressure mismatch.

Nomenclature

AoA	Angle of Attack
AFC	Active Flow Control
CFJ	Co-Flow Jet
$FASIP$	Flow-Acoustics-Structure Interaction Package
LE	Leading Edge
TE	Trailing Edge
$RANS$	Reynolds-Averaged Navier-Stokes
$ZNMF$	Zero-Net Mass Flux
P	CFJ pumping power, $P = \frac{\dot{m}C_pT_{t2}}{\eta}(\Gamma^{\frac{\gamma-1}{\gamma}} - 1)$
η	CFJ pumping system efficiency, propeller efficiency
P_c	Power coefficient, $P_c = \frac{P}{\frac{1}{2}\rho_\infty V_\infty^3 S}$

* Ph.D. Candidate
† Ph.D. Student
‡ Post-doctoral Researcher
§ Professor, AIAA associate Fellow

PR	Total pressure ratio, Γ
C_L	Lift coefficient
C_{Lmax}	Maximum lift coefficient
C_D	Drag coefficient
C_μ	Jet momentum coefficient, $C_\mu = \frac{\dot{m}V_j}{\frac{1}{2}\rho_\infty {V_\infty}^2 S}$
R_e	Reynolds number
Ma	Mach number
C_p	Pressure coefficient
c_p	Constant pressure specific heat
γ	Air specific heats ratio
S	Planform area of the wing
ρ_∞	Freestream density
V_∞	Freestream velocity
T_t	Total temperature
P_t	Total pressure
H_t	Total enthalpy
α	Angle of attack
$\dot{m}$	Mass flow
C	Chord length
$_j$	Subscript, stands for jet

1 Introduction

Co-flow jet (CFJ) airfoil utilizes active flow control (AFC) to achieve high lift and aerodynamic efficiency enhancement at low energy expenditure [1, 2, 3, 4, 5, 6, 7, 8, 9, 10, 11]. As sketched in Fig. 1, a CFJ airfoil draws a small amount of mass flow into the airfoil near the trailing edge, pressurizes and energizes it using a micro-compressor actuator embedded inside the airfoil, and then tangentially injects the mass flow near the leading edge. The CFJ airfoil does not add any mass flow to the airfoil system and thus is a zero-net-mass-flux (ZNMF) system.

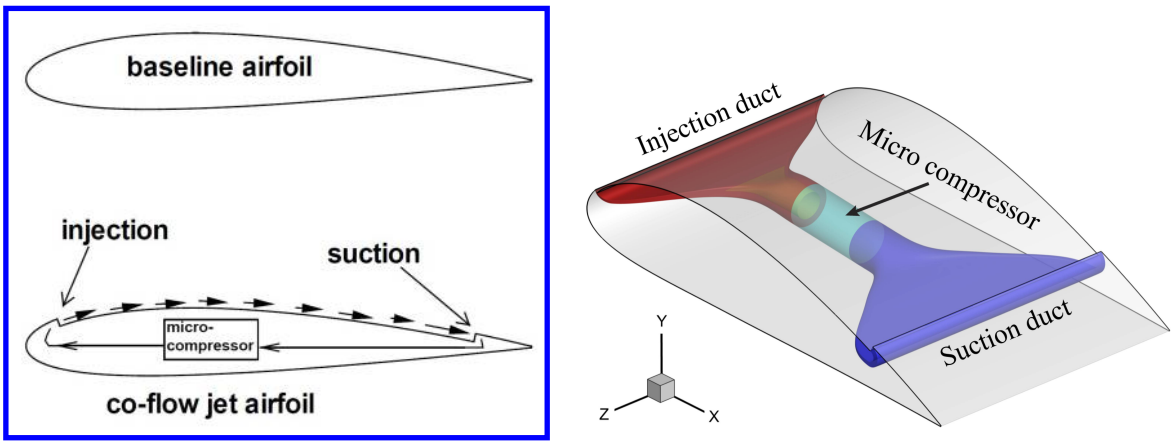

(a) 2D sketch (b) 3D sketch

Figure 1: Sketches of a CFJ Airfoil with micro-compressor embedded

In 2017, Yang and Zha [5] numerically obtained an airfoil lift coefficients exceeding the theoretical limit using CFJ active flow control based on Reynolds Averaged Navier-Stokes (RANS) equations. A lift coefficient greater than the theoretical limit, $C_{Lmax} = 2\pi(1 + t/c)$, is termed a Super-Lift Coefficient (SLC) [5]. In 2018, Xu et al [12, 13, 14] applied the CFJ flow control to an aircraft control surface, which demonstrates a very high control authority enhancement. Recently, a CFJ airfoil wind tunnel experiment [15] is conducted with embedded micro-compressors. It is the first time that a CFJ airfoil is successfully controlled by the self-contained zero-net mass-flux (ZNMF) system, which is a crucial step to bring the CFJ airfoil to practical aerospace applications. The study experimentally proved that a CFJ airfoil can achieve the SLC exceeding the theoretical limit of potential flow theory.

However, during the wind tunnel testing, the micro-compressors did not work along the designed operating line as desired. Instead, the compressors are pushed to an operating line at choked condition [15]. It is because the mismatch between the low pressure at the CFJ airfoil leading injection location and the high outlet pressure of the micro-compressors. It reduces the efficiency of the CFJ system from about 80% to a low value of about 25%. The mismatch is because the micro-compressors are designed separately from the CFJ airfoil via a loose boundary condition interface determined by CFD simulation. The details of the off-design operation are not clear due to lack of experimental measurement. Therefore, it is important to simulate and understand the CFJ injection and suction ducts and micro-compressor as an integrated system to guide future design.

The purpose of this paper is to numerically simulate the micro-compressor performance with integrated injection and suction ducts to understand the off-design operation of the micro-compressor during the wing tunnel testing. Such simulation is an important step to develop the integrated design process to make the CFJ airfoil with the embedded micro-compressors actuators to operate along the design operating line and achieve high operating efficiency.

2 The Tested CFJ Airfoil

The tested CFJ-NACA-6421 airfoil has 5 embedded micro-compressors and 5 sets of injection and suction ducts as shown in Fig. 2 [15]. The simulation is conducted in ANSYS CFX using 3D Reynolds Averaged Navier-Stokes (RANS) CFD calculation with the viscous effects simulated by the k-ϵ model. The boundary conditions are directly adopted from the wind tunnel testing to mimic the experimental conditions.

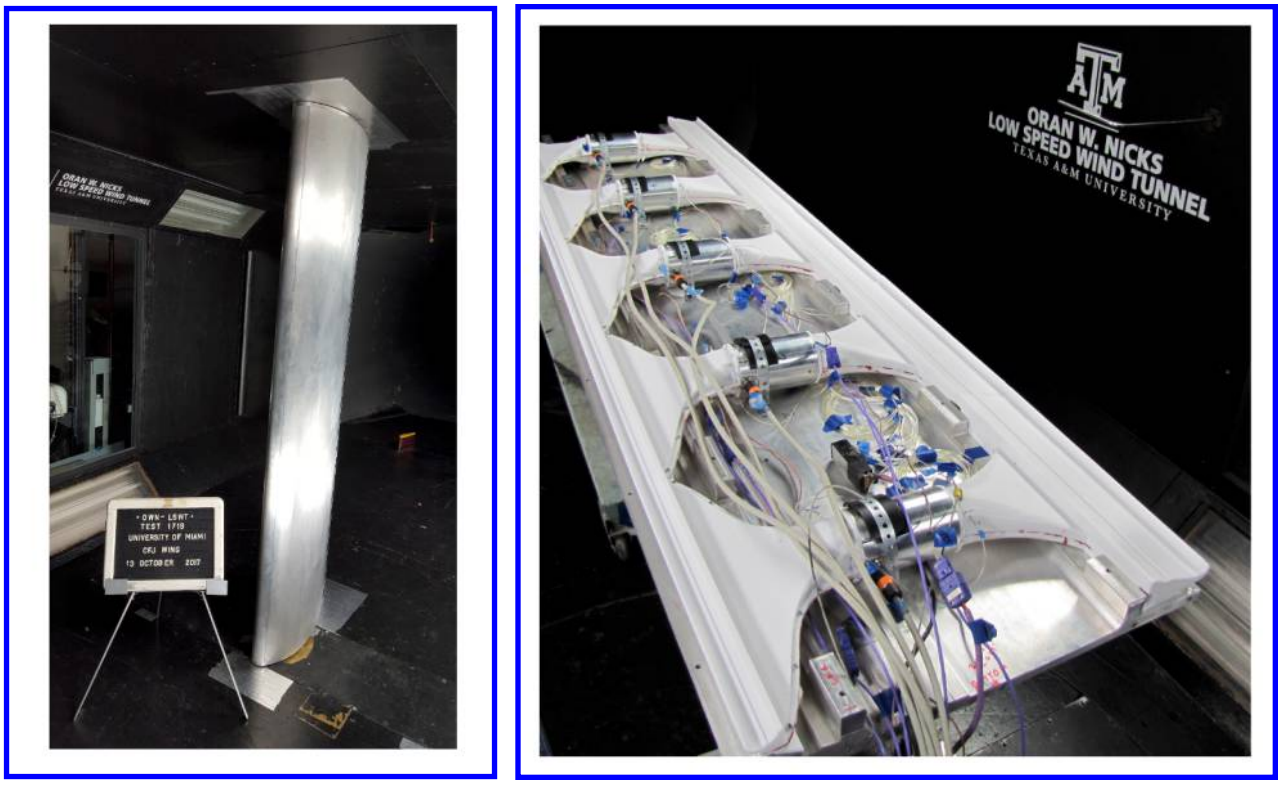

(a) Tested CFJ airfoil (b) CFJ Airfoil with 5 embedded micro-compressors

Figure 2: Photos of the CFJ-NACA-6421 airfoil [15]

As shown in Fig. 3, the mixed-flow micro-compressor consists of a converging intake, an impeller, a diffusor and a deswirl OGV and an outlet duct. It is designed at 115000 rpm with the design point total pressure ratio of 1.21 and isentropic efficiency of 80.2%. Fig. 4 presents the computed results and experimental measurements of the micro-compressor performance, which are in an excellent agreement.

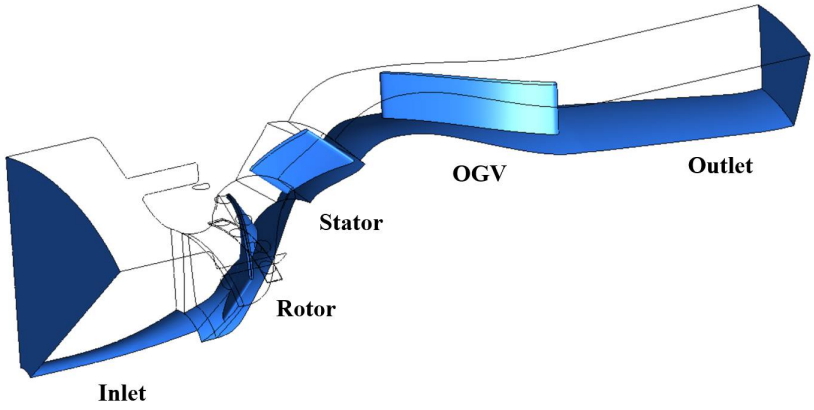

Figure 3: Configuration of the validated micro-compressor

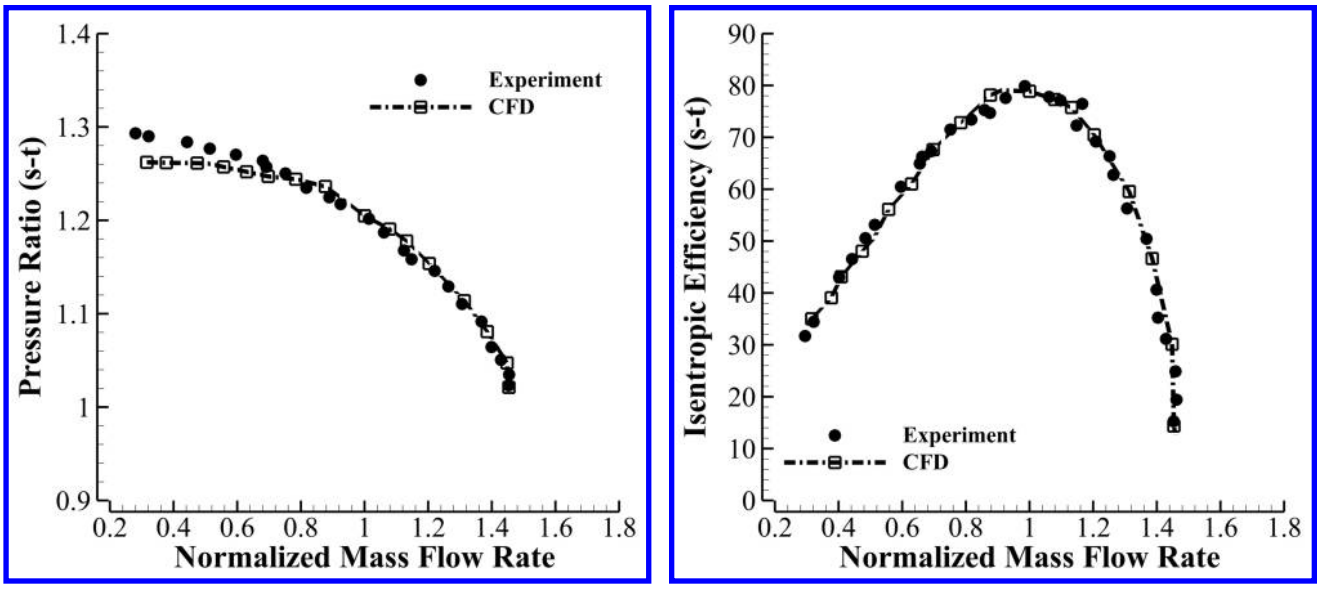

(a) Pressure ratio (b) Isentropic efficiency

Figure 4: Computed speedlines of a micro-compressor compared with the measured results [16]

Fig. 5 shows the geometry of injection and suction ducts designed by Yan and Zha [17] and manufactured by 3D-printing. Their cross sections are transformed from circular to rectangular shape. Different from the suction duct, the injection duct has a center body as shown in Fig. 5 (a), which is used to guide the swirl flow coming out of the micro-compressor to prevent flow separation.

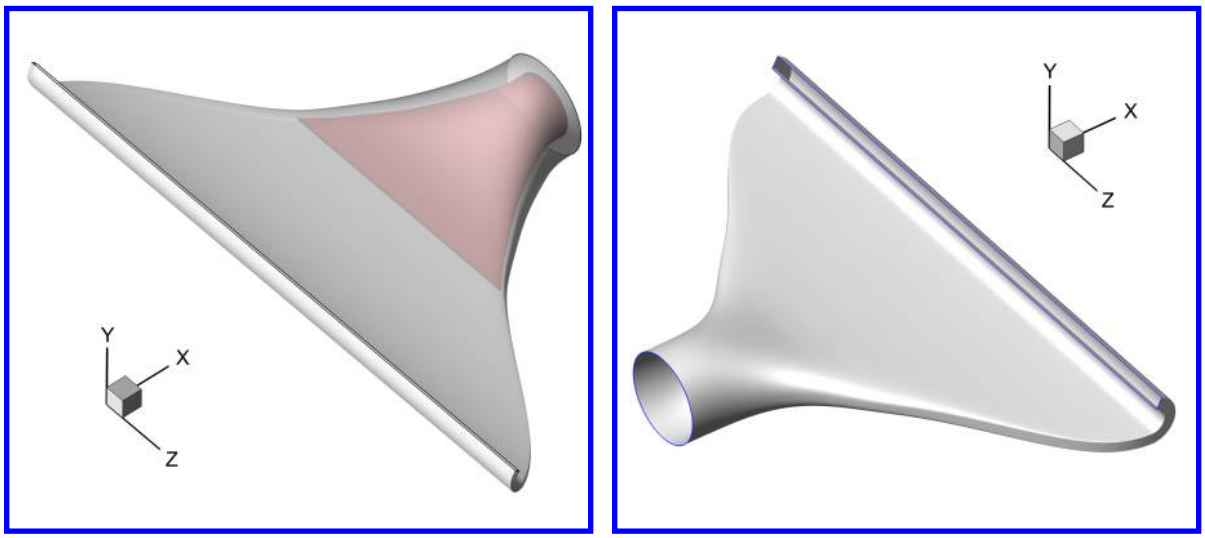

(a) Injection duct (b) Suction duct

Figure 5: Geometry of the injection and suction ducts [17]

The streamlines and flow fields of the injection and suction ducts designed to cruise at Mach 0.15 are shown in Fig. 6 [17]. For the injection duct, the flow at two sides of the center body is stronger than it is at bottom and top due to the swirl effects. The 2D Mach number contour slices in Fig. 6 (b) show the flow is nicely attached at various injection duct span. Overall, the injection and suction ducts are well designed and flow is very attached

through out the ducts [17].

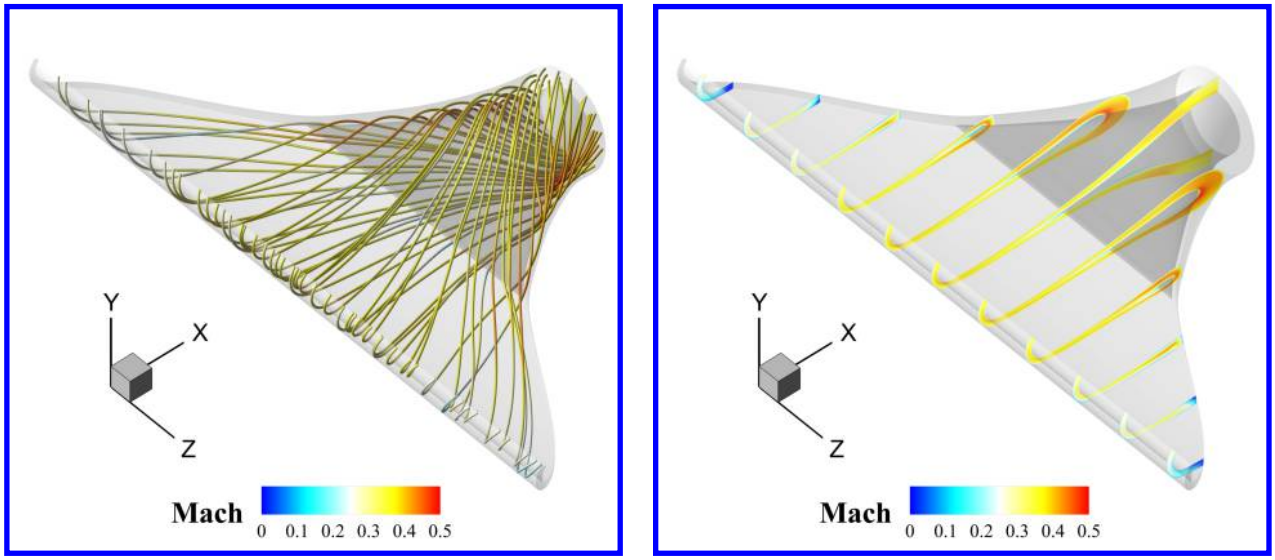

(a) Streamlines of the injection duct (b) Spanwise Mach contours of the injection duct

Figure 6: Flow fields of the injection duct [17]

2.1 Micro-compressor Map Operating Line

At the wind tunnel testing, each micro-compressor has a total pressure and static pressure probes at the compressor inlet and outlet. Three of the five compressors also have the temperature sensors at the inlet and outlet. The intent is to help to determine the mass flow rate and pressure ratio of the compressor. However, since the flow has high swirl at the compressor (about 60°) outlet, the total pressure measurement is not reliable. The compressor map is hence plotted as compressor outlet static pressure to the compressor inlet total pressure as shown in Fig. 7, which is measured in the rig test [16]. The design operating line (in blue) is intended to go through the peak efficiency region with the efficiency value of 80% . However, in the wind tunnel testing for the CFJ airfoil conducted by Zha et al in [15], the actual operating line that the micro-compressors work is pushed to a position with substantially lower pressure ratio shown as the thick dark line near the bottom of the compressor map, which gives an averaged efficiency of 25%.

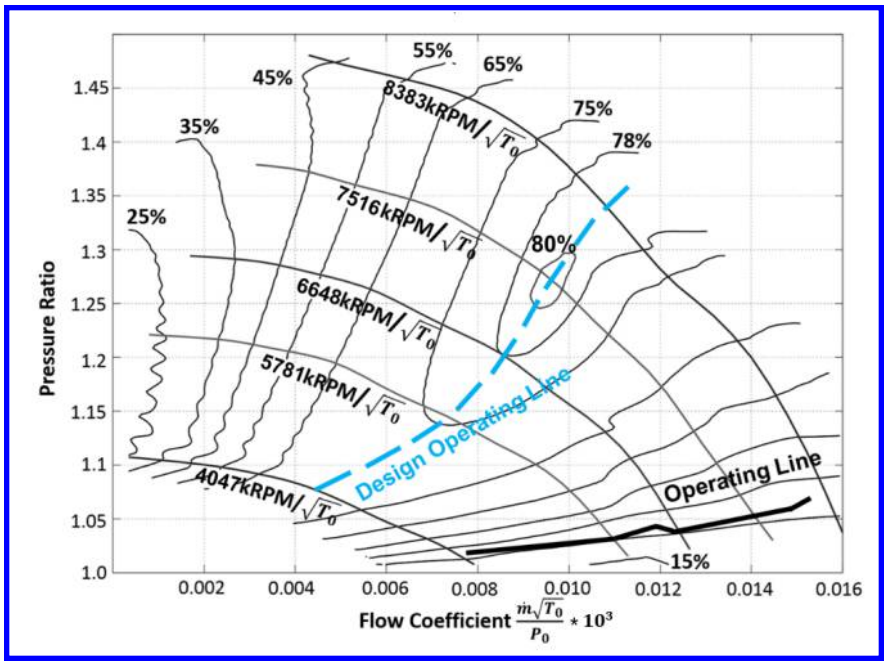

Figure 7: Measured micro-compressor operating line

The reason for the large shift of the operating line is that there is a mismatch between the low pressure ratio required by the CFJ airfoil and the high pressure ratio provided by the micro-compressors. Referring to the 3D sketch of the CFJ airfoil in Fig. 1, the mismatch is mostly because the design of the CFJ airfoil, injection and suction ducts (in purple and deep blue) and the micro-compressors (light blue) are conducted separately. They are linked by boundary conditions of each component without a tight integration.

The ideal design process is to simulate the integrated CFJ airfoil, injection and suction ducts, and the micro-compressor all together at the same time. But it will be very costly and have long turn-around time. A less direct way is to iterate two integrated subsystems: 1) the CFJ airfoil with the injection and suctions ducts; 2) the micro-compressor with the injection and suction ducts. This design process will have the injection and suction duct as the common parts of the two subsystems, which will be iterated in the design to match the CFJ airfoil required performance. Ren and Zha [18] conducted the simulation of the subsystem 1 with the CFJ airfoil integrated with 3D injection and suction ducts. The present work is to develop the subsystem 2 with the micro-compressor integrated with the injection and suction ducts.

3 Simulation of the Micro-compressor integrated with the Ducts

This section describes the simulation process of the micro-compressor integrated with ducts including the computational domain and boundary conditions set-up. The flow fields will be discussed in detail and the computed micro-compressor performance will be compared with the measured operating line.

3.1 Simulation Method

The ANASYS CFX CFD code solving Reynolds Averaged Navier-Stokes (RANS) equations with the k-ϵ turbulence model is used for the simulation. The computational domain is displayed in Fig. 8, which includes a suction duct, an injection duct and a single passage of the micro-compressor with an intake, an impeller, a stator and an OGV outlet. Since the CFJ suction duct is symmetric for both the flow and geometry, only half of the suction duct is simulated with symmetry boundary condition to save the computational resources. However, the symmetry boundary condition is not used for the injection duct because the swirl from the compressor outlet makes the flow lose the symmetry. The total pressure inlet and static pressure outlet boundary conditions are applied at suction duct inlet and injection duct outlet respectively. The mixing interface boundary conditions are used on the interfaces between blade rows and the interface between the micro-compressor and the CFJ injection and suction ducts. The total mesh size is 6.3 million nodes. The convergence criterion is that the residual reduced by 4 orders of magnitude.

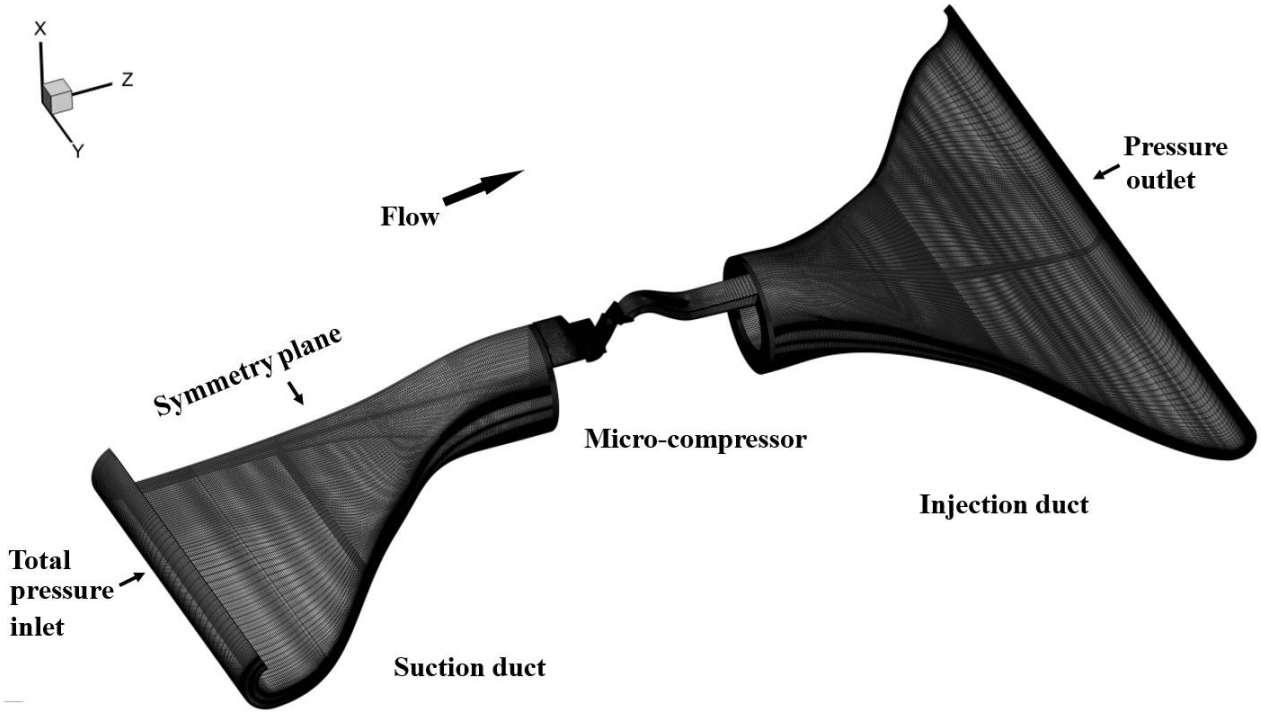

Figure 8: Computational domain of the micro-compressor and ducts simulation

3.2 Results and Discussions

The micro-compressor and CFJ ducts simulation is conducted for five different RPMs. In each RPM, the experimental data of the total pressure and static pressure are utilized at suction duct inlet and injection duct outlet to simulate the experimental operating condition. Table 1 shows the boundary condition details of the 5 cases.

Table 1: Boundary conditions measured in the experiment [15]

Cases	RPM	V_∞ (m/s)	Suc duct inlet P_t (Pa)	Suc duct inlet T_t (K)	Inj duct outlet P_s (Pa)
1	75000	9.355	100359	309.44	101395
2	100000	9.289	100359	309.44	102753
3	115000	9.346	100359	309.44	103745
4	126700	9.143	100359	309.44	104780
5	135000	9.113	100359	309.44	105066

Case 3 is at the design RPM and is used in this paper for the detail discussion. Fig. 9 shows the Mach number contours of three span locations of micro-compressor impeller. The maximum Mach number near the rotor tip is below 0.7 and the rotor is not choked. The flow in the impeller rotor has a little separation. However, downstream the impeller, the stator blade has a high negative incidence that flow separation occurs at the lower span on the pressure surface as shown in Fig. 10.

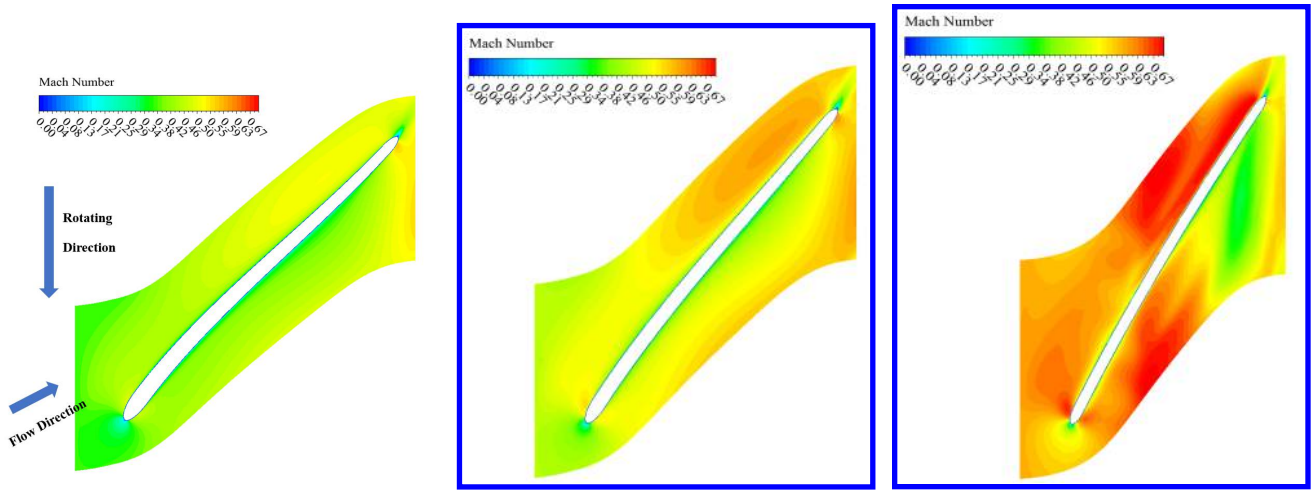

(a) Span 10% (b) Span 50% (c) Span 95%

Figure 9: Rotor blade spanwise Mach contours

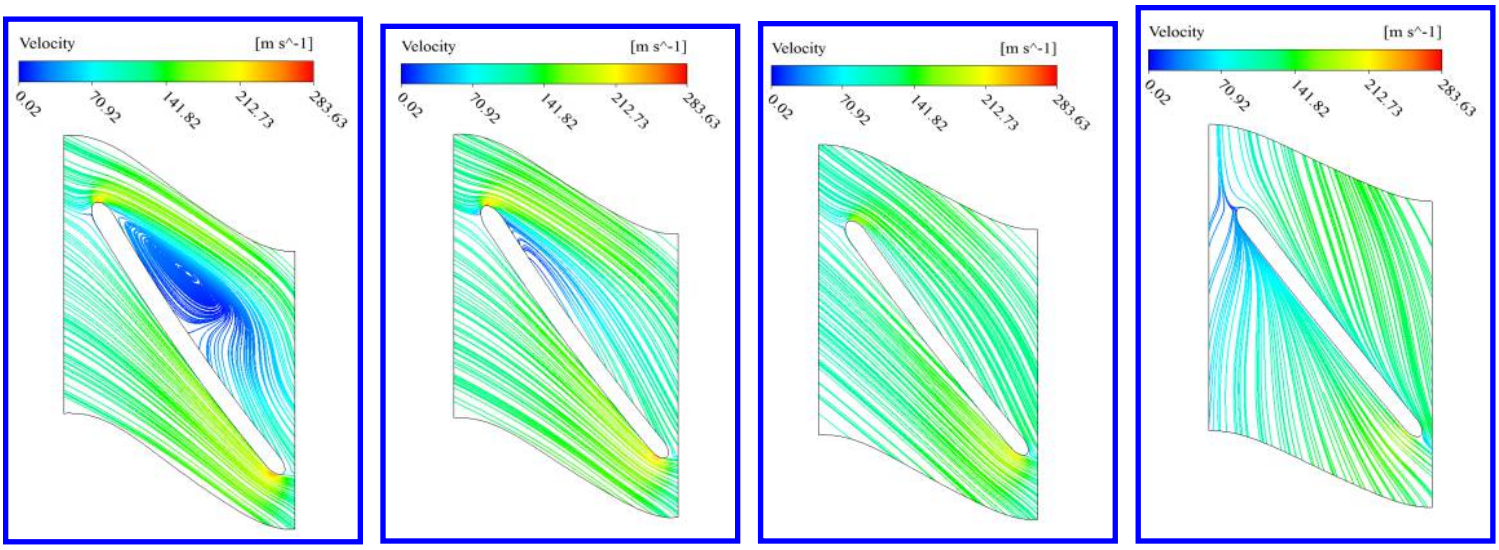

(a) Span 25% (b) Span 50% (c) Span 75% (d) Span 95%

Figure 10: Stator blade spanwise streamlines

Fig. 11 shows the streamwise and spanwise 2D Mach contours of the CFJ injection duct. It is observed that, the flow close to the center body has lower velocity than near the injection duct casing. As the flow approaches downstream, the flow is mixed and becomes more uniform. Fig. 12 displays the simulation of the integrated system with the pressure contours on the micro-compressor and the streamlines colored by static pressure in the injection and suction duct. No apparent flow separation is observed as designed [17] in Fig. 6.

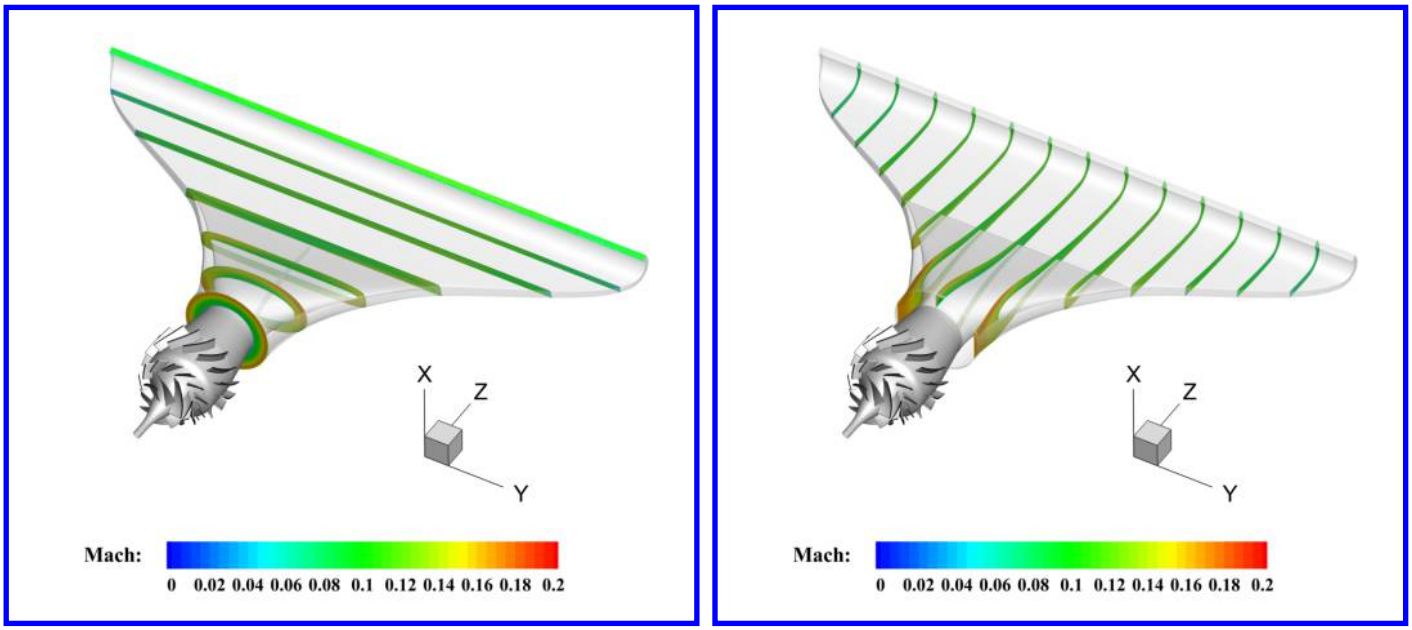

(a) Streamwise Mach number contours (b) Spanwise Mach number contours

Figure 11: Flow fields of the injection duct connected with the micro-compressor

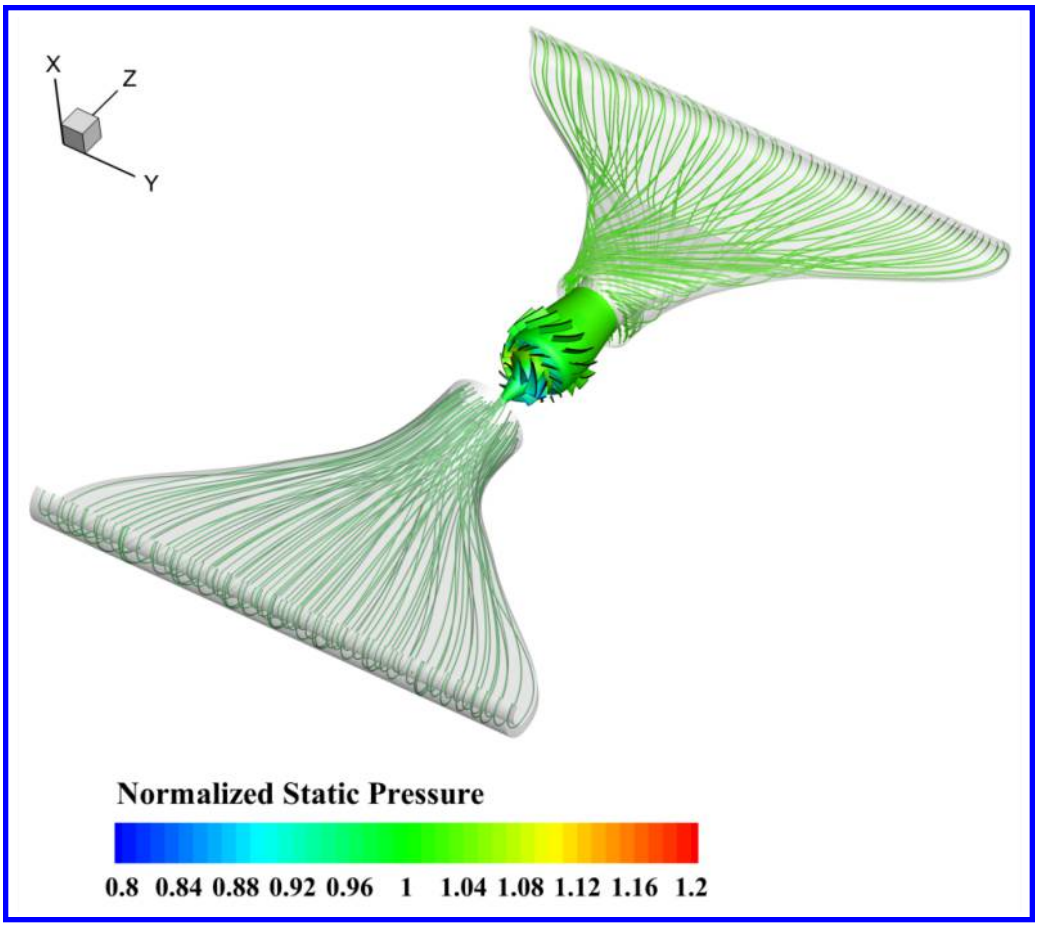

Figure 12: Simulated streamlines of the injection and suction ducts and the pressure contours of the micro-compressor

Fig. 13 presents the streamwise and spanwise Mach contours of the suction duct. The similar centrifugal effect observed in the designed suction duct in [17] is also observed here as the bottom flow is stronger than the flow near the top surface.

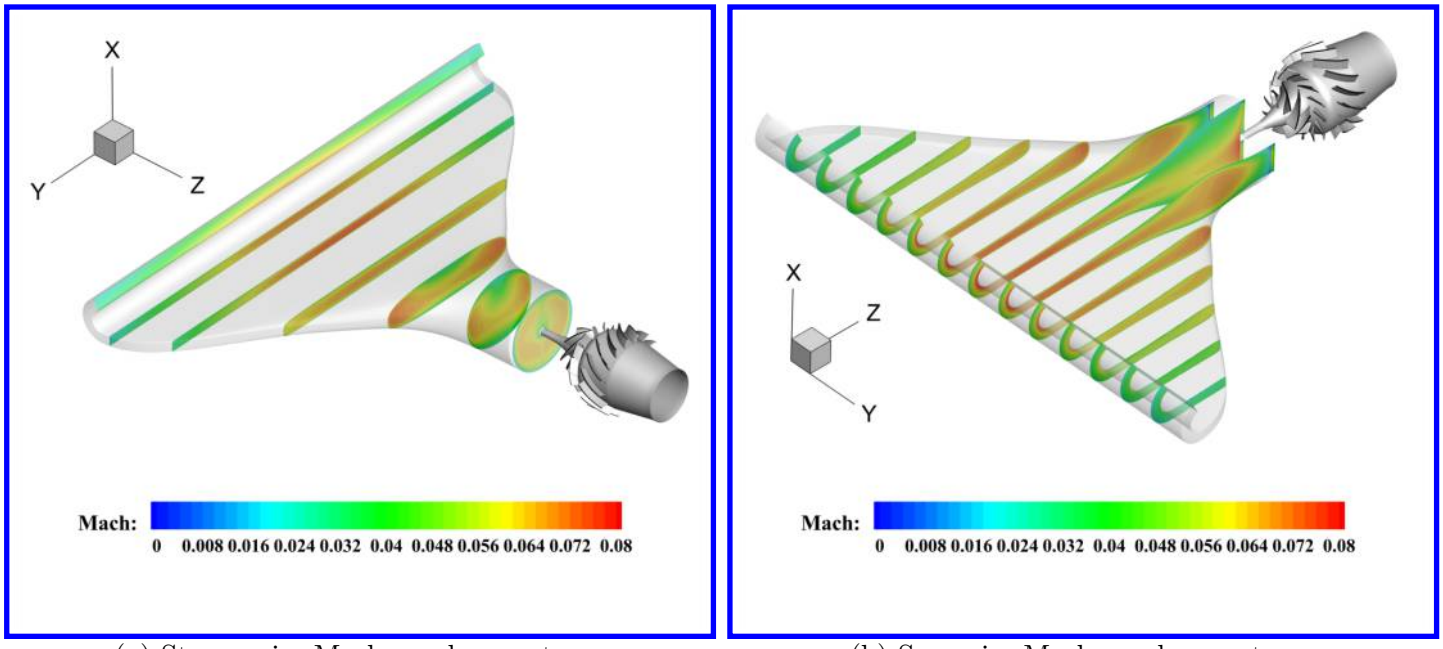

(a) Streamwise Mach number contours (b) Spanwise Mach number contours

Figure 13: Flow fields of the suction duct connected with the micro-compressor

Table 2 presents the compressor performance and calculated C_μ and P_c for the five simulated cases. The computed pressure ratio and isentropic efficiency for the cruise condition are plotted on the measured compressor map as shown in Fig. 14. A good agreement of pressure ratio is achieved between wind tunnel testing and simulation with the maximum discrepancy of 3%, which indicates that the simulations mimic the experiment very well.

Table 2: Calculated micro-compressor performance in various RPM

Cases	RPM	Mass flow rate (kg/s)	P_{s-t} (Pa)	η_{s-t}	C_μ	P_c
1	75000	0.047	1.020	0.197	0.077	0.0006
2	100000	0.062	1.040	0.239	0.130	0.0015
3	115000	0.070	1.054	0.249	0.168	0.0023
4	126700	0.077	1.069	0.261	0.218	0.0034
5	135000	0.082	1.075	0.246	0.237	0.0038

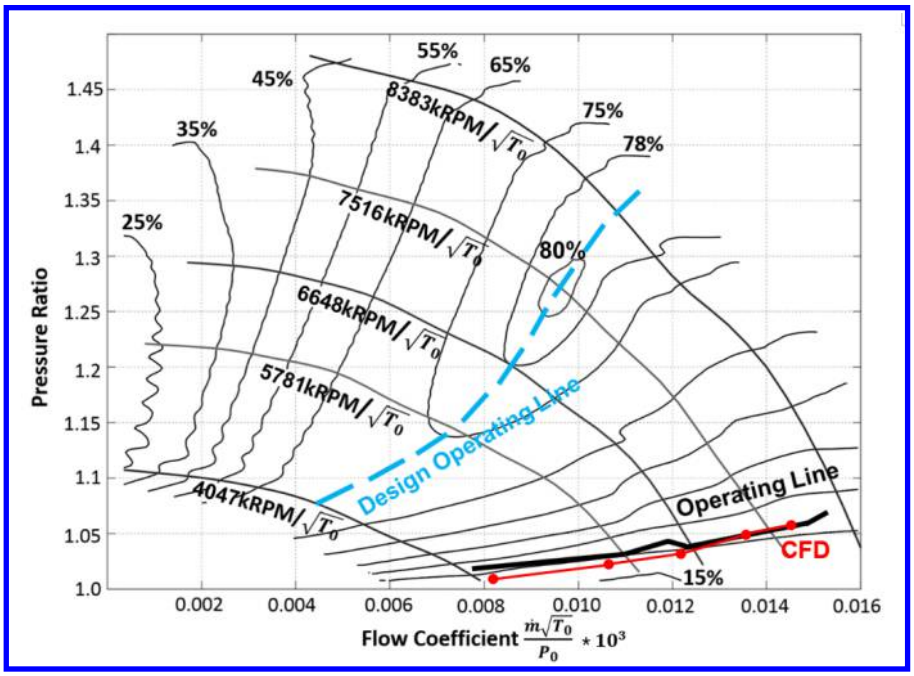

Figure 14: Predicted and measured micro-compressor map

Fig. 14 indicates that the compressor-CFJ ducts system is operated at the off-design condition with a low pressure ratio. The reason is the pressure mismatch between the micro-compressor back pressure and the static pressure at the CFJ injection duct outlet [15]. The micro-compressor provides a high back pressure of 1.2 atm for the design point operation, but the static pressure of the injection duct outlet required by the CFJ airfoil is less than 1 atm due to the super-suction effects, which pushes the compressor to operate at a low pressure ratio. However, the compressor is not choked with the highest Mach number occurring near the rotor tip region and is below 0.7 as indicated in Fig. 9.

The possible solutions to resolve the pressure mismatch include: 1) Redesign the micro-compressor with a lower back pressure so that the compressor can work at the static pressure required by the CFJ injection slot; 2) Keep a high pressure ratio for the micro-compressor, but redesign the injection duct to a converging shape to reduce the back pressure at the CFJ airfoil injection slot. However, the latter will require a highly converging duct, which will increase the outlet Mach number and energy loss. For a CFJ airplane cruising at subsonic Mach number, the micro-compressor with a lower total pressure ratio and higher mass flow rate is required to achieve high efficiency. This means the present micro-compressor needs to be redesigned to achieve lower pressure ratio and higher mass flow rate. Redesigning the micro-compressor to meet the requirements of the CFJ airfoil working at a broad range of Mach number up to transonic flow is necessary and is pursued by Xu and Zha in [19, 20].

4 Integrated Design Process

An integrated design process of ducts and micro-compressor is proposed to avoid the pressure mismatch between the CFJ airfoil and the micro-compressors. As shown in Fig. 15, the integrated design process involves three separated aerodynamic design processes: 1) CFJ airfoil or wing design, 2) micro-compressor (MC) design, and 3) CFJ injection and suction ducts design. The CFJ areo-design is first conducted to specify the targeted operating conditions of the CFJ wing for the whole flight envelop including the coefficient of lift, drag, pitching moment at

take-off/landing and cruise. During this process, the 3D ducts must be simulated with the CFJ wing (Fig.16 (a)). In the first process, the CFJ aerodynamic performance will require a certain performance from the micro-compressor (i.e. pressure ratio, mass flow rate, efficiency), which will be imposed as the boundary conditions, including the compressor outlet profiles (i.e. radial distribution of swirl, total pressure, total temperature, etc) and compressor inlet profile (i.e. radial distribution of static pressure) [18]. The required micro-compressor performance in the first process will be used as the targeted performance to design the micro-compressor.

The second process is to design the micro-compressor with the injection and suction duct as shown in Fig.16 (b). The CFJ aerodynamic performance in the first process will determine a certain flow profiles on the injection slot and suction slot (i.e. velocity, mass flow rate, static pressure, etc.). These flow field profiles will be imposed as the boundary conditions at the very inlet and outlet of the compressor-duct system as shown in Fig.16 (b). To satisfy the specified boundary conditions, the micro-compressor needs to reach a certain performance. If the micro-compressor performance provided in the second process does not match the micro-compressor performance required in the first process, the design will start a new iteration and be repeated until they match. In reality, since the micro-compressor design takes a long time, the micro-compressor design will be frozen after one or two iterations. The design iteration will be mostly to vary the duct geometry and CFJ airfoil geometry to deliver the required CFJ system aerodynamic performance. At the end of the integrated design process, it is desirable to conduct a final design verification with the simulation of the whole integrated system of the CFJ airfoil, ducts and micro-compressor.

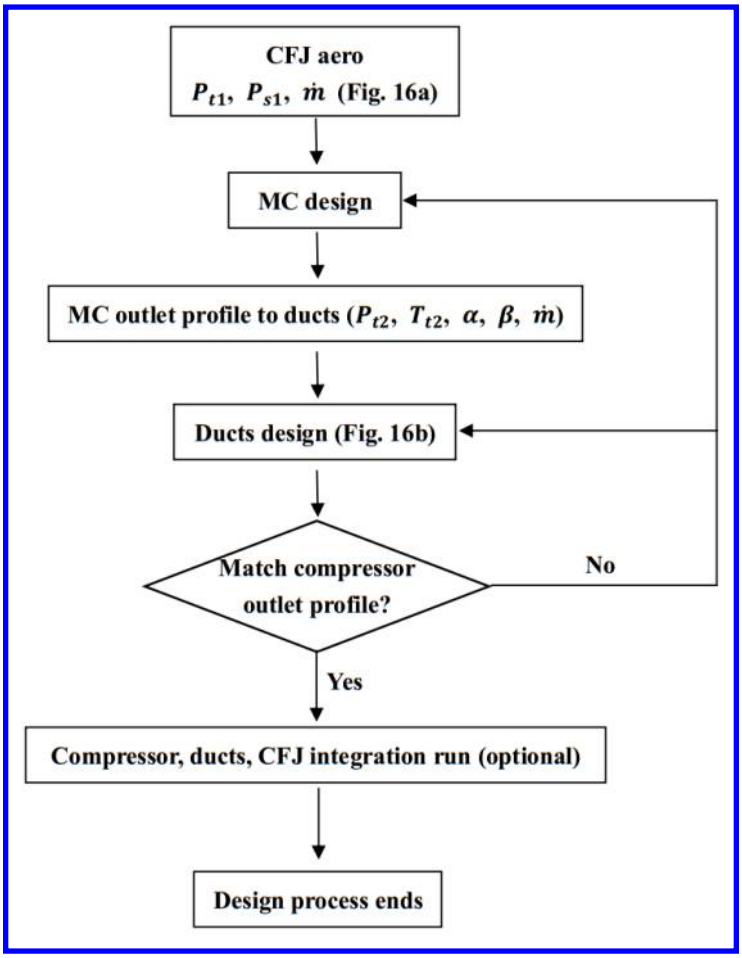

Figure 15: Flow chart for the integrated design process

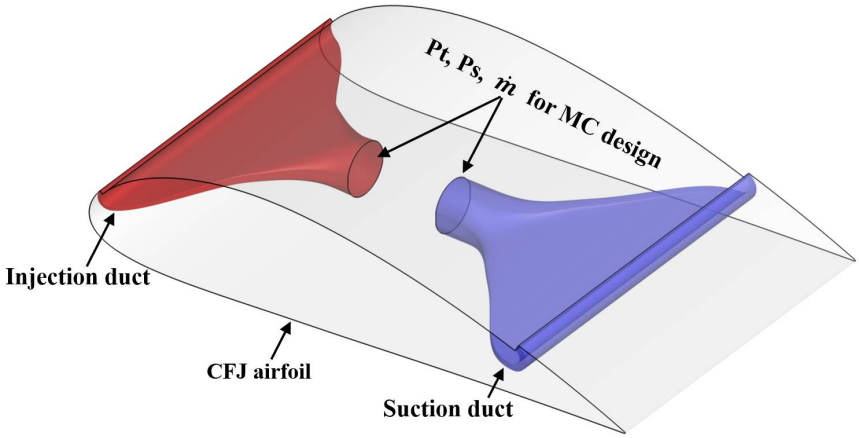

(a) CFJ areo design process

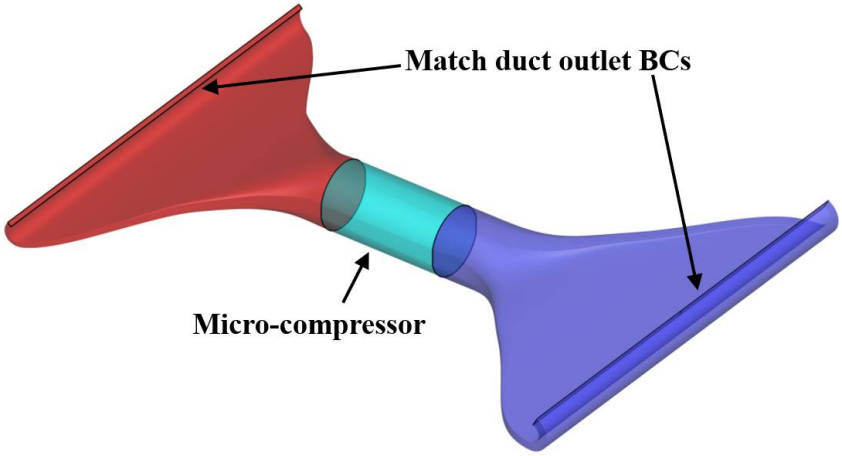

(b) Duct design process

Figure 16: Illustration of the integrated design process

5 Conclusion

The off-design operation of the micro-compressor used in a CFJ airfoil wind tunnel testing is numerically studied in the present paper. It is found that the micro-compressors are operated at an operating line that is shifted from the design operating line with substantially lower pressure ratio. This is because that the static pressure at the CFJ airfoil injection area near leading edge is very low due to the very strong suction effect caused by the CFJ injection effect. Such off-design operation is caused by the CFJ airfoil with the injection ducts and micro-compressors designed with a loose integration, which creates the mismatch between the compressor provided back pressure and the static pressure required by the CFJ injection duct outlet. The micro-compressor is over-designed to have a too high back pressure at the design point. To avoid the pressure mismatch, an integrated design process is proposed involving three separated aerodynamic design processes: 1) CFJ airfoil or wing design, 2) micro-compressor (MC) design, and 3) CFJ injection and suction ducts design. These three design processes will be integrated by two sub-systems: 1) the CFJ airfoil/wing with the injection and suction ducts; 2) the micro-compressor with the

injection and suction ducts. The ducts are used as the bridge to connect the design of CFJ airfoil and the design of micro-compressor, and iterate the two designs until they both reach the targeted performance. This study is an important step to develop an integrated design process that avoids the pressure mismatch for the future design.

6 Acknowledgment

The simulations are conducted on Pegasus super-computing system at the Center for Computational Sciences at the University of Miami.

Disclosure: Dr. GeCheng Zha is on the Board of Directors/Corporate Officer for Co-flow Jet and holds equity in Co-flow Jet. Dr. Zha is also the inventor of intellectual property licensed to Co-flow Jet.

References

[1] Zha, G.-C and Paxton, C. and Conley, A. and Wells, A. and Carroll, B., "Effect of Injection Slot Size on High Performance Co-Flow Jet Airfoil," *AIAA Journal of Aircraft*, vol. 43, 2006.

[2] Zha, G.-C and Carroll, B. and Paxton, C. and Conley, A. and Wells, A., "High Performance Airfoil with Co-Flow Jet Flow Control," *AIAA Journal*, vol. 45, 2007.

[3] B. P. E. Dano, G.-C. Zha, and M. Castillo, "Experimental Study of Co-Flow Jet Airfoil Performance Enhancement Using Micro Discreet Jets." AIAA Paper 2011-0941, 49th AIAA Aerospace Sciences Meeting, Orlando, FL,, 4-7 January 2011.

[4] Lefebvre, A. and Dano, B. and Bartow, W. and Di Franzo, M. and Zha, G.-C., "Performance and Energy Expenditure of Co-Flow Jet Airfoil with Variation of Mach Number," *AIAA Journal of Aircraft*, vol. 53, pp. 1757–1767, 2016.

[5] Yang, Y.-C. and Zha, G.-C., "Super-Lift Coefficient of Active Flow Control Airfoil: What Is the Limit?." AIAA Paper 2017-1693, AIAA SCITECH2017, 55th AIAA Aerospace Science Meeting, Grapevine, Texas, 9-13 January 2017.

[6] Zha, G.-C. and Gao, W. and Paxton, C., "Jet Effects on Co-Flow Jet Airfoil Performance," *AIAA Journal, No. 6,*, vol. 45, pp. 1222–1231, 2007.

[7] G.-C. Zha and D. C. Paxton, "A Novel Flow Control Method for Airfoil Performance Enhancement Using Co-Flow Jet." *Applications of Circulation Control Technologies*, Chapter 10, p. 293-314, Vol. 214, Progress in Astronautics and Aeronautics, AIAA Book Series, Editors: Joslin, R. D. and Jones, G.S., 2006.

[8] Wang, B.-Y. and Haddoukessouni, B. and Levy, J. and Zha, G.-C., "Numerical Investigations of Injection Slot Size Effect on the Performance of Co-Flow Jet Airfoil ," *AIAA Journal of Aircraft*, vol. 45, pp. 2084–2091, 2008.

[9] B. P. E. Dano, D. Kirk, and G.-C. Zha, "Experimental Investigation of Jet Mixing Mechanism of Co- Flow Jet Airfoil." AIAA-2010-4421, (5th AIAA Flow Control Conference, Chicago, IL), 28 Jun - 1 Jul 2010.

[10] Lefebvre, A. and Zha, G.-C. , "Design of High Wing Loading Compact Electric Airplane Utilizing Co-Flow Jet Flow Control." AIAA Paper 2015-0772, AIAA SciTech2015: 53nd Aerospace Sciences Meeting, Kissimmee, FL, 5-9 Jan 2015.

[11] Liu, Z.-X. and Zha, G.-C., "Transonic Airfoil Performance Enhancement Using Co-Flow Jet Active Flow Control." AIAA Paper 2016-3472, AIAA AVIATION 2016, 8th AIAA Flow Control Conference, Washington, D.C, June 13-17, 2016.

[12] X. Kewei and G. Zha, "High control authority 3d aircraft control surfaces using co-flow jet," *AIAA Aviation and Aeronautics Forum and Exposition 2019*, 2019.

[13] J. Zhang, K. Xu, Y. Yang, Y. Ren, P. Patel, and G. Zha, "Aircraft control surfaces using co-flow jet active flow control airfoil," in *June 25-29,2018 Applied Aerodynamics Conference, Atlanta, Georgia*, AIAA 2018-3067.

[14] K. Xu, J. Zhang, and G. Zha, "Drag minimization of co-flow jet control surfaces at cruise conditions," in *AIAA Scitech 2019 Forum*, AIAA 2019-1848.

[15] G.-C. Zha, Y.-C. Yang, Y. Ren, B. McBreen, E. White, and L. Brown, "Experimental study of super-lifting and thrusting airfoil of coflow jet actuated by micro-compressors." AIAA AVIATION 2018, Atlanta, GA , AIAA Paper-2018-3061.

[16] C. Zwyssig, "Design of a mixed flow fan prototype," in *Internal Report to University of Miami*, vol. PR-4241-011, Celereton, Oct. 24, 2017.

[17] Y. Ren and G. Zha, "Design of injection and suction ducts for co-flow jet airfoils with embedded micro-compressor actuator," in *June 25-29, 2018 Flow Control Conference, Atlanta, Georgia*, AIAA 2018-3062.

[18] Y. Ren and G. Zha, "Simulation of 3d co-flow jet airfoil with embedded micro-compressor actuator," in *2018 AIAA Aerospace Sciences Meeting*, AIAA Paper 2018-0330.

[19] X. Kewei and G. Zha, "Improving efficiency of co-flow jet micro-compressor actuator outlet guide vanes and nozzle," *AIAA Science and Technology Forum 2019,Applied Aerodynamics Conference*, 17-21 June, 2019, Hilton Anatole, Dallas, Texas.

[20] X. Kewei and G.-C. Zha, "Design of High Specific Speed Mixed Flow Micro-Compressor for Co-flow Jet Actuators." ASME Paper GT2019-90980, ASME TURBO EXPO 2019, Phoenix, Arizona, USA, June 17-21, 2019.